Chemosphere 376 (2025) 144272

Contents lists available at ScienceDirect

Chemosphere

journal homepage: www.elsevier.com/locate/chemosphere

Geochemical characterization of groundwater and source apportionment of potential pollutants in a tribal stretch infected with chronic kidney disease of unknown etiology

Herojeet Rajkumar [a], Pradeep K. Naik [b,*,1], Rakesh K. Dewangan [b], Janak R. Verma [b], Prabir K. Naik [b]

[a] Department of Environmental Studies, Post Graduate Government College, Sector-11, Chandigarh, 160011, India
[b] Central Ground Water Board, North Central Chhattisgarh Region, Ministry of Jal Shakti, Govt. of India, LK Corporates Tower, Dumartarai, Dhamtari Road, Raipur, 492015, India

HIGHLIGHTS

- Comprehensive Water Quality Index classifies 52% of the water samples as potable.
- Rock-water interactions and cation exchange are the dominant reaction processes.
- Strong correlation between Cl^- and NO_3^- ions reflects anthropogenic contamination.
- Carbonates, anhydrite, gypsum, and calc-silicates give higher $Ca^{2+} + Mg^{2+}$ ions.
- Hardness ($Ca^{2+} + Mg^{2+}$), increased Na^+/Ca^{2+} ratio and F- ions possibly induce CKDu.

GRAPHICAL ABSTRACT

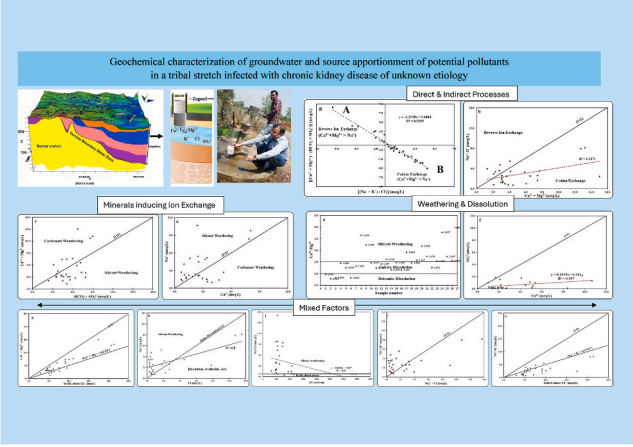

ARTICLE INFO

Keywords:
Aquifers
Hydrochemistry
Rock-water interactions
Fluoride
CKDu
Supebeda

ABSTRACT

This paper draws world attention toward a tribal stretch in central India exposed to chronic kidney disease of unknown etiology (CKDu). To date, about 100 people have died and more than 300 hospitalized from a single village, Supebeda, of 1200 inhabitants. The occurrence of CKDu in this part of the world is a recent discovery and its potential pollutants are still eluding human understanding. Since groundwater is being accused as the culprit, this contribution attempts to characterize the area geochemically, study major rock-water interactions, identify potential pollutants, and apportion their sources. Analytical results of 27 groundwater samples reveal that the area suffers from NO_3^- (0–128.3 mg/L) and F^- (0–1.9 mg/L) contamination with total hardness, Ca^{2+}, Mg^{2+}, and

* Corresponding author.
E-mail address: pradeep.naik@water.net.in (P.K. Naik).
[1] Present Address: Centre for Hydrological Sciences and Communication, C3/37, Kendriya Vihar, Tamando, Bhubaneswar 751028, India. ORCID: 0000-0001-7576-2980.

https://doi.org/10.1016/j.chemosphere.2025.144272
Received 23 September 2024; Received in revised form 27 February 2025; Accepted 28 February 2025

Cl^- as other violator parameters. Comprehensive Water Quality Index classifies ~52% of the samples as potable; ~37% could be suitable for drinking pending certain treatment. While elevated F^- concentrations are due to the weathering of fluoride-bearing minerals (fluorite, amphiboles, biotite, hornblende, granite gneiss, etc.), the excess Ca^{2+} and Mg^{2+} ions are attributed to 63% of the samples exhibiting cation exchange processes (Ca^{2+}, Mg^{2+}, $Cl^- < Na^+ + K^+$) resulting from the weathering of carbonate (calcite, dolomite), anhydrite, gypsum, calc-silicate (anorthite, plagioclase, amphiboles) and ferromagnesian (hornblende, biotite) minerals in the metamorphic rocks. About 22% of the samples depict reverse ion exchange processes (Ca^{2+}, Mg^{2+}, $Cl^- > Na^+ + K^+$) due to silicate weathering including dissolution of Cl^- salts (albite and halite minerals) and anthropogenic inputs that also contribute to elevated concentrations of NO_3^-.

1. Introduction

Chronic kidney disease (CKD) has emerged as the third fastest-growing health malady infecting about 850 million people worldwide (Nature, 2024). From a fatality rank of 16 in 2016, it rose to the rank of 12 in 2017 in just a year's span with a global mortality rate of 1.2 million deaths per annum (GBD-CKDC, 2020). By the year 2040, it is predicted to become the fifth highest cause of years of life lost with an annual mortality rate of 2.2–4 million people globally (Foreman et al., 2018). The disease CKDu (Chronic Kidney Disease of Unknown Etiology) is the most enigmatic in the extensive list of CKD variants, with no common consensus on its origin. With no precise clinical features encompassing all attributes of the disease or globally standardized diagnostics criteria, even the world body of Kidney Disease Improving Global Outcomes (https://kdigo.org/), which develops and implements evidence-based clinical practice guidelines for the prevention and treatment of kidney diseases, remains silent on its etiology. What is common worldwide, however, is the type of human community it predominantly infects, i.e., the low-income agricultural workers in the vulnerable segments of society, particularly in the low-and lower-middle-income countries in Africa, Asia, and South America (Bradley et al., 2024; Fiseha et al., 2024). Since chronic kidney diseases impose the highest economic burden of any disease group in the world (Essue et al., 2018; Levin et al., 2023), the economic turmoil in the CKDu affected families in these countries can very well be imagined.

Many workers attribute CKDu to several causative factors, such as water, overuse of pesticides, heat stress, strenuous labor, dehydration, overuse of non-steroidal anti-inflammatory drugs, mycotoxins, hypertension, infections, diabetes mellitus, herbal medication, family history, tobacco use, etc. (Anupama et al., 2020; Stalin et al., 2020; Hettithanthri et al., 2021; Jolly and Thomas, 2022; Priyadarshani et al., 2023). Of late, groundwater is being singled out by several workers as the primary factor for CKDu's origin, such as in Sri Lanka (Imbulana and Oguma, 2021; Zeng et al., 2022; Shi et al., 2023; Chandrajith et al., 2024), India (Khandare et al., 2015; Mascarenhas et al., 2017; Tatapudi et al., 2019; Lal et al., 2020) and central America (Campese, 2017). Recently, Nayak et al. (2023) from the Indian Council of Medical Research attribute CKDu to water and agricultural farming based on 25 case studies conducted around the world. The present contribution too investigates a case where groundwater is accused of CKDu's progression.

The study pertains to the village Supebeda in a tribal stretch in the Gariabandh district of Chhattisgarh State, central India where more than 100 people have already died and over 300 compulsively hospitalized due to CKDu (Chowdhary et al., 2020). Numerous media reports and a public outcry erupted abruptly in the region calling for the Government's attention in 2018. Since the entire population in the village depends on groundwater for all their water needs, people complained of its contamination. The present team investigated the area from a hydrogeological perspective in 2020 to allay their apprehension (Dewangan and Verma, 2022). Although the preliminary examination did not divulge any serious quality deterioration, further analyses by Herojeet et al. (2023) did reveal nitrate (NO_3^-) and fluoride (F-) contamination. These results were supported by a joint study conducted by various regional hospitals, including the premier All India Institute of Medical Sciences (AIIMS) on CKDu (John et al., 2021). Medical reports showed elevated concentrations of urinary fluoride in CDKu patients; some even exhibited radiological features of skeletal fluorosis (Chowdhary et al., 2020), accusing F^- as one of the primary etiological factors. Attempt was made, therefore, to find the sources of F^- besides a few other violator parameters, such as total hardness (TH), Ca^{2+}, Mg^{2+} and Cl^-. This necessitated detailed geochemical investigations involving groundwater and the aquifers through which water emerges for public usage as drinking water.

Groundwater contains a wide variety of inorganic constituents in dissolved state because of chemical interactions with host rocks and contributions from the atmosphere. Therefore, the study of geochemistry is of prime importance in deciding about the quality of water and evaluating the hydrogeochemical processes responsible for temporal and spatial changes in the chemistry of groundwater (Mukherjee and Singh, 2022). In fact, hydrochemical results provide a basis for characterizing groundwater within the aquifers and from this information, it is possible to draw inferences concerning the processes that may be occurring within the host rocks (Şen, 2015). In this context, although groundwater has been blamed for CKDu's propagation in the Supebeda region, its chemistry in terms of rock-water interactions giving rise to potential pollutants is poorly examined. The AIIMS and a few other medical institutions did carry out some research in the area, but their studies are mostly from epidemiological and community health perspectives (Chowdhary et al., 2020; John et al., 2021; Rathore et al., 2022; Galhotra et al., 2023). The present contribution, quite different from these studies, aims at the geochemical characterization of groundwater including analysis of major rock-water interactions, identification of potential pollutants and their source apportionment through various statistical techniques in the Supebeda region.

The work has been divided into several sections. This Introduction section presents the context of this study, while the section on 'Materials and Methods' describes the study area, local geology and hydrogeological features as well as the water sampling and analytical procedures. The section on 'Results and Discussion' makes a geochemical evaluation of groundwater resources from a potability perspective and classifies the groundwater samples based on specific ion concentrations and base exchange indices. Further, it does source apportionment of the potential pollutants based on several geochemical signatures arising out of rock-water interactions through direct and indirect processes, weathering and dissolution, and mixed factors, such as geogenic and anthropogenic sources. Finally, the paper briefly discusses the link between hydrogeochemistry and CKDu in the study area. These primary studies on the geochemical characterization of groundwater in affected area including source apportionment of the potential pollutants are essential to understand in depth the etiological features of CKDu for greater good of humanity.

Elsewhere in India, CKDu has been reported in the states of Odisha (Mohanty et al., 2020), Andhra Pradesh (Ramesh et al., 2011; Ganguli, 2016; Lal et al., 2020), Maharashtra (Mogal, 2020), Tamil Nadu (Parameswaran et al., 2020), Goa (Mascarenhas et al., 2017), and Delhi (Ghosh et al., 2017). Most of the studies conducted in these states are from medical and water quality perspectives with limited geochemical emphasis. The present contribution is a full-scale hydrogeochemical

work with a focus on rock-water interactions carried out for the first time in the country. In no other CKDu area in the world, hydrogeochemistry based on rock-water interactions has ever been studied to such a greater magnitude, which makes this work unique globally.

2. Materials and methods

2.1. Study area

The village Supebeda lies in a tribal stretch in the Gariabandh District of Chhattisgarh State, India (Fig. 1). With a population of 1200 people, the village has a geographical area of 3 km^2 adjoining the river Tel that demarcates its border with the eastern State of Odisha. It has a nearly equal male-female sex ratio and a literacy rate of 50.51%. Agriculture is the primary occupation of people. Many are farm laborers working on a daily wage basis; some do cattle grazing. Rathore et al. (2022) give a detailed account of the food habits of the people living in the village. The region is characterized by the subtropical monsoon type of climate with an annual rainfall of 1200 mm. Winter temperature varies between 5 °C and 25 °C and that of summer between 29 °C and 46 °C.

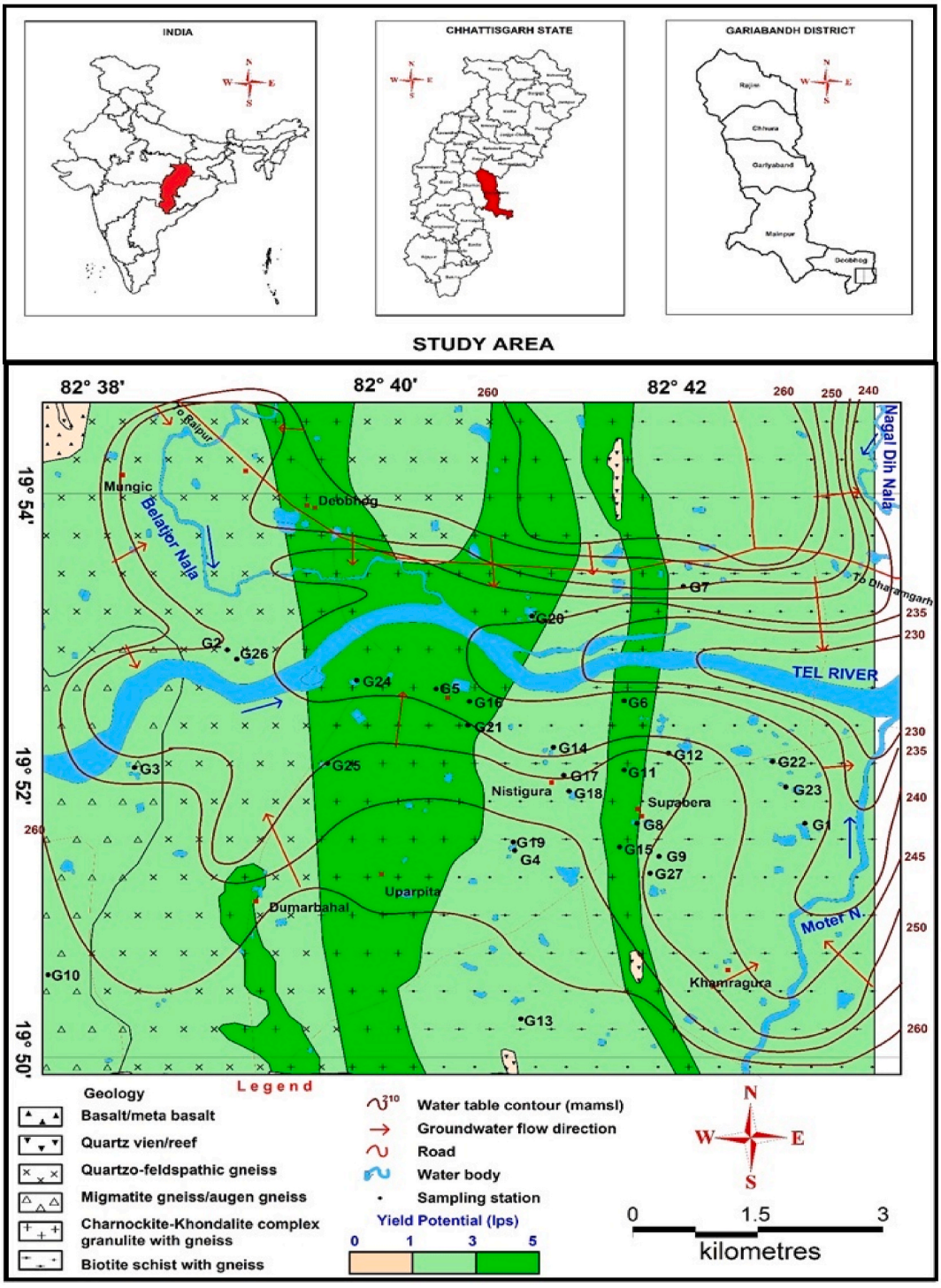

Fig. 1. Sampling locations and hydrogeology in the village Supebeda, district Gariabandh, Chhattisgarh State, India.

2.2. Local geology

Geologically, the area consists of three lithological units: (i) migmatiticquartzo feldspathic gneiss, (ii) banded augen gneiss, and (iii) hornblende granite (Gupta et al., 2000; Neogi and Das, 2000) (Fig. 1). The grey-colored, medium-grained migmatiticquartzo feldspathic gneisses comprises of finely laminated alternations of felsic (quartz + plagioclase + K-feldspar: Qtz + Pl + Kfs) and mafic (Biotite + Hornblende: Bt + Hbl-rich) bands. Leucocratic segregations are conspicuous and are stromatically folded into or parallel to the layerings. Orthopyroxenes as greasy, green patches with diffuse margins ('patchy charnockite') occur occasionally. Band of migmatized mafic granulites, metapelitic rocks (infrequently sapphirine-bearing), and rare calcsilicate granulites occur concurrently besides isolated appearances of blastoporphyritic charnockite.

The medium-to coarse-grained banded augen gneisses are pink-colored with bandings within them defined by the mafic and felsic layers of K-feldspar (Kfs) augen and quartz lenticels. Closer to the migmatitic quartzofeldspathic gneiss unit, leucosomes occur occasionally in narrow zones with a sharp abetment toward the west. The gneissic fabric generally precedes the leucosomes. Hornblende (Hbl-rich) and plagioclase + clinopyroxene (Pl + Cpx-rich) layers occur thinly within the banded gneisses. With these thin layers, amphibolites (Hornblende + plagioclase ± granite ± clinopyroxene: Hbl + Pl ± Grt ± Cpx) and calcsilicate gneisses are mesoscopic to the regional scale bands.

Pink-colored, coarse-grained hornblende granite consisting of microcline, quartz, hornblende, and biotite intrude into the banded gneiss. This unit is characterized by intense shearing and mylonitization along its eastern fringe and has a poor westward occurrence.

2.3. Hydrogeology

Hydrogeology of the study area is mainly controlled by geological setup and surface slope conditions. The composition and structure of geological formations influence the inherent properties such as porosity and permeability and hence the water holding and water yielding capacity of the aquifers. Groundwater occurs under unconfined conditions at shallower levels in the weathered portions of the rocks up to about 20 m depth, while semi-confined to confined conditions occur in deeper aquifers beyond a depth of 30 m (Fig. 1). Rainfall is the primary source of recharge in the shallow unconfined aquifers; other recharge sources include the water bodies, such as tanks, canals, and streams. Groundwater discharge sources from these aquifers include groundwater abstraction by humans, evapotranspiration and baseflow. Groundwater movement at shallower levels follows the surface topography and is generally directed toward the topographic lows and valleys. The groundwater elevation contours (240–260 m) depict the regional groundwater movement toward the E-W flowing Tel River from both North and South (Fig. 1); the perennial nature of the river proves this. Dugwells are prevalent in shallow aquifers with a depth range of 7–16 m and a yield range of 25–40 m^3/day (Dewangan and Verma, 2022).

Semi-confined to confined conditions prevail in the fractured zones at depth, especially in the charnockite and khondalite (CGWB, 2001). The water receiving or yielding capacity in these formations largely depends on the extent of fracturing, openness and size of fractures and their interconnection with the near surface weathered zones. These deeper aquifers are tapped by borewells of 50–80 m depth with a yield capacity of about 85–430 m^3/day (Dewangan and Verma, 2022). Fracture zones through which most groundwater movement takes place are encountered at 40–45, 60–65, and 75–80 m depth (CGWB, 2022). Transmissivity ranges between 15 and 45 m^2/day in charnockite and khondalite and occasionally goes up to 100 m^2/day (CGWB, 2023). The primary source of discharge from these aquifers is groundwater abstraction.

2.4. Water sampling and analysis

One pair of groundwater samples in 1000 ml HDPE plastic bottles were collected from 27 scattered locations from the wells during the pre-monsoon season (May 2020) (Fig. 1). The bottles were prewashed with HNO_3 (10%) and rinsed with double-deionized water. Before sampling, stored groundwater at each location was pumped out for 10–15 min to get fresh solutions, and sampling bottles were thoroughly rinsed 2–3 times with fresh groundwater. Chemical parameters, such as pH and EC were measured onsite using Digital pH and Conductivity meters (make WTW, Model inoLab® pH 7110) with an accuracy of ±0.1. The parameter TDS was calculated by multiplying the factor 0.64 with EC value (μS/cm) of the respective groundwater samples. The samples were then filtered using the Whatman filter paper (0.45 μm) to remove suspended particulate matter. The samples were acidified with HNO_3 (pH ~2) and kept at 4 °C to retain their natural character.

Standard protocols (APHA, 2005), approved by the National Accreditation Board for Testing and Calibration Laboratories (NABL), the Constituent Board of Quality Council of India, were adopted in the laboratory for analysis of major cations (Ca^{2+}, Mg^{2+}, Na^{+}, and K^{+}) and anions (HCO_3^-, Cl^-, SO_4^{2-}, F^-, and NO_3^-). Total Hardness (TH) and Ca^{2+} were determined by complexometric EDTA Titration method. Magnesium was calculated by the difference of the total hardness (TH) and calcium (TH – Ca^{2+}) concentrations. The chemical parameters, Na^{+} and K^{+}, were determined using Flame Photometer (Make Systronic, model 128). The bicarbonate (HCO_3^-) was measured by an acid base titration method. Chloride (Cl^-) concentration was analyzed by volumetric titration with silver nitrate. The parameters, SO_4^{2-} and NO_3^-, were determined by Spectrophotometer (UV–Vis Motras Scientific) and F^- was analyzed by Ion Selective Electrode (make Thermo Fisher, Model Orion 4 star) by using TISAB-3 solution.

Strict measures were taken to avoid contamination of the water samples. Merck-GR grade chemicals and reagents were used to prepare chemical solutions using double-deionized water. All glassware and apparatus were soaked with 10% hydrochloric acid (HCl) for one day and cleaned with double-deionized water. Blank samples were prepared from the stock solutions of each parameter for instrumental calibration. The reference standards certified by the National Institute of Standards and Technology (NIST) of the United States Department of Commerce were used for calibration of the instruments. The samples were analyzed three times based on the procedures defined by the APHA (2005) and approved by the NABL, India. Instrumental calibration was done with standard and blank samples for every 10 samples to ensure efficiency and maintain accuracy of all experimental data. Finally, the analytical accuracy was examined using the charge balance error (CBE) equation with an acceptable limit of ±5% (Hounslow, 2018) (Eq. (1), Table S1).

$$\mathrm{CBE\%} = \frac{\sum (Cations) meq/L - \sum (Anions) meq/L}{\sum (Cations) meq/L + \sum (Anions) meq/L} \times 100 \quad (1)$$

3. Results and discussions

3.1. Hydrochemistry

Appraisal for the suitability of Supebeda's groundwater for drinking purposes has been made with the help of standards defined by the Bureau of Indian Standards (BIS) (2020) and World Health Organization (WHO) (2022). All analytical data of the physicochemical parameters are listed in Table S1 and their descriptive statistics in Table 1, which also lists the percentage and number of samples exceeding the BIS and WHO limits, shown also in Figs. S1 (a - m). All these tables and figures are self-explanatory.

Groundwater in the Supebeda area is slightly alkaline in nature (pH 7.9 ± 0.3). While 11% of the samples exceed the WHO guideline EC value of 1500 μS/cm, in the case of Total Dissolved Solids (TDS), 25.93% of the samples exceed the BIS acceptable limit of 500 mg/L excluding

Table 1
Descriptive statistics of the physicochemical parameters of the groundwater samples from the village Supebeda, Gariabandh District, Chhattisgarh State, India.

Parameter	Premonsoon Season (May 2020)			BIS (2020) Standards		% of sample above the BIS (2020) and WHO (2022) Standards		Undesirable Effects	References
	Minimum	Maximum	Mean ± SD	AL	PL	AL<PL	PL>AL		
Physical parameters									
pH	7.2	8.3	7.9 ± 0.3	6.5–8.5		NIL		Low pH: bitter metallic taste, corrosion high pH: slippery feel, soda taste, deposits, affects mucous membrane	BIS (2020); USEPA (2024)
EC	313.0	3446.0	941 ± 795	1500[a]		11.11% (3)		Laxative effect	BIS (2020)
TDS	200.32	2205.44	602.2 ± 509.0	500	2000	25.93% (7)	7.41% (2)	Gastrointestinal irritation, hardness; deposits, colored water, staining, salty taste	BIS (2020); USEPA (2024)
TH	65.0	755.0	257 ± 178	200	600	33.33% (9)	11.11% (3)	Calcification of arteries, urolithiasis, anencephaly, and gastrointestinal tract irritation	Sidhu et al. (2013); Singh et al. (2020a,b)
Major cations									
Ca^{2+}	20.0	214.0	67 ± 53	75	200	29.63% (8)	3.70% (1)	Kidney ailments, bladder problems, urination disorder, and scale formation	BIS (2020); Singh et al. (2020a,b)
Mg^{2+}	3.6	52.8	21 ± 13.2	30	100	18.52% (5)	NIL	Laxative effect	BIS (2020); Singh et al. (2020a,b)
Na^{+}	16.4	185.5	65 ± 43.9	200[a]		NIL		High blood pressure	BIS (2020)
K^{+}	0.6	11.4	2.2 ± 2.1	12[a]		NIL		Bitter taste, laxative effects on human digestive and nervous systems	BIS (2020); Singh et al. (2020a,b)
Major anions									
HCO_3^-	85.0	519.0	297 ± 109	500[a]		3.7% (1)		–	–
Cl^-	7.1	408.3	73.8 ± 109.2	250	1000	11.11% (3)	NIL	Affects kidney function, heart problem, and salty taste	BIS (2020); CAWST (2009); USEPA (2024)
SO_4^{2-}	4.8	105.5	29 ± 30.6	200	400	NIL	NIL	Excess sulphates of magnesium or sodium may cause a laxative effect, gastrointestinal irritation, cathartic effect. May cause salty taste in water	Singh et al. (2020a,b); CDC (2020)
NO_3^-	0	128.3	39 ± 40	45		37.04% (10)		Methemoglobinemia or blue baby syndrome	BIS (2020); WHO (2022); CAWST (2009); USEPA (2024)
F^-	0	1.9	0.9 ± 0.6	1	1.5	14.81% (4)	25.93% (7)	Staining and pitting in teeth and problems in joints and bones; Discoloration of teeth; kidney dysfunction	BIS (2020); WHO (2022); CDC (2020); USEPA (2024); Quadri et al. (2018); Zuo et al. (2018)

Abbreviations: AL = acceptable limit. PL = permissible limit in the absence of an alternative source of water.
[a] Guideline value as per WHO (2022) since BIS (2020) does not provide any limit for this parameter.

7.41% the permissible limit of 2000 mg/L. With regard to total hardness (TH), about 44.44% of the samples exceed the BIS-acceptable limit of 200 mg/L including 11.11% the permissible limit of 600 mg/L. Higher hardness could be due to the presence of significant amount of alkaline earths (Ca^{2+} and Mg^{2+}) and weak acid (HCO_3^-) in groundwater (Herojeet et al., 2016; Sunkari et al., 2020; Rajkumar et al., 2025a). Ca^{2+} is the most dominant cation with 33.33% of the samples showing concentrations above the BIS acceptable limit of 75 mg/L, while in the case of Mg^{2+}, about 18.52% of the samples exceed their acceptable limit of 30 mg/L. The alkali metals (Na^+ and K^+) are within their respective prescribed acceptable limits.

Among the anions, bicarbonate (HCO_3^-) is the most dominant and in the case of Cl^-, 11.11% of the samples exceed its BIS acceptable limit of 250 mg/L. While SO_4^{2-} is within the prescribed limit of 200 mg/L, elevated concentrations of HCO_3^- and Cl^- along with excess alkaline earths (Ca^{2+} and Mg^{2+}) tend to increase the hardness in groundwater. Weathering and dissolution of silicate, carbonate (calcite, dolomite), gypsum and sandstone minerals as well as leaching from agrochemicals from the agricultural fields could be the possible reasons (Singh et al., 2020a; Zhou et al., 2020 Liu et al., 2021; Herojeet et al., 2023). Numerous anthropogenic activities, such as domestic wastewater, livestock waste, agriculture runoff, septic tank seepages, and application of Cl^- fertilizers (viz., ammonium chloride and potash) too may be contributing to the higher amount of Cl^- in groundwater (Zhou et al., 2014; Karunanidhi et al., 2021; Rao et al., 2022).

Supebeda suffers from both NO_3^- and F^- contamination. The NO_3^- concentration varies between 0 and 128.3 mg/L with a mean ± SD of 39 ± 40 mg/L, and 37% of the samples exceed the BIS permissible limit of 45 mg/L. While excess NO_3^- has many health effects, its primary sources could be numerous anthropogenic activities, such as excreta from livestock farms, runoff from agricultural land, leaching from waste dumping sites, and discharge of untreated domestic sewerage lines in a typical village environment (Rao et al., 2022; Das et al., 2023; Awaleh et al., 2024; Rajkumar et al., 2025b). The F^- concentration varies between 0 and 1.9 mg/L with a mean ± SD of 0.9 ± 0.6 mg/L. About 41% of the samples exceed their acceptable limit of 1.0 mg/L including 26% of the samples their permissible limit of 1.5 mg/L. Weathering of fluoride-bearing minerals, such as fluorite, amphiboles, biotite, hornblende granite gneiss, etc., in rocks, sediments, and soils, evapotranspiration and atmospheric depositions could be the reason for the elevated concentrations of F^- (Awaleh et al., 2024; Shaji et al., 2024; Tiwari et al., 2020).

3.2. Groundwater quality based on Comprehensive Water Quality Index (CWQI)

The newly developed water quality index (CWQI) (Rajkumar et al., 2022) was applied to validate the suitability appraisal of groundwater for various uses based on the prescribed limits defined by the BIS (2020) and WHO (2022). Table S2 shows that the positive CWQI score, i.e., P_{CWQI}, ranges between 0.14 and 0.61 and that of negative CWQI (N_{CWQI}) between (−0.78) – 0.00. Out of the six different classes CWQI defines, 22% of the samples fall into 'excellent' water class, 56% into 'good', 11% into 'marginal' and another 11% into 'very poor' (Table S3, Fig. S2). While water samples constituting the 'excellent' water class can be consumed directly for drinking, the samples under 'good' category can

be conditionally used for the same purpose. They are safe, however, for other domestic uses. Few of these samples (G1, G4, G8, G14, G15, G20, G21) have a single violator parameter with F^- level exceeding the maximum permissible limit of 1.5 mg/L. Groundwater at these locations could be used for drinking only after proper onsite treatment. The commonly available defluoridation methods are reverse osmosis, nanofiltration, electrodialysis, and membrane distillation, and ion exchange processes. Nutritious food with optimum amounts of calcium and vitamin C help prevent F^- related problems (Maitra et al., 2021). The 11% of the samples (G19, G22, and G26) under the marginal water class too could be used for drinking after adequate treatment. These samples could be used, however, for other domestic needs. The rest 11% of the samples (G17, G18, and G25) under 'very poor' category are neither good for drinking nor for domestic uses, but could be utilized for agricultural purposes, especially for salt-tolerant crops.

The method CWQI is very robust that uses regulatory limits of both relaxable and non-relaxable chemical parameters. The groundwater samples in this method are classified based on the quality rating and unit weight of each physicochemical parameter. Therefore, water classification coming out of CWQI is highly reliable (Herojeet et al., 2023).

3.3. Groundwater characterization

3.3.1. Hydrochemical facies

The Piper diagram (Fig. S3) depicts that the groundwater of the area is mainly dominated by alkaline earths over alkalis and weak acids over strong acids (Piper, 1944). Three dominant hydrochemical facies are predominant, viz., Ca^{2+}-Mg^{2+}-$HCO3^-$ (55.56%), Ca^{2+}-Mg^{2+}-Cl^--SO_4^{2-} (29.63%), and Na^+-K^+-HCO_3^- (14.81%). The groundwater samples could be further categorized into four distinct water classes, such as Ca^{2+}-HCO_3^- (55.56%), Ca^{2+}-Cl^- (7.40%), Ca^{2+}-Mg^{2+}-Cl^- (22.22%), and Ca^{2+}-Na^+- HCO_3^- (14.81%). The cation triangle shows that the majority (70.37%) of the samples do not belong to any dominant chemical zone, and the remaining 11.11%, 14.82%, and 3.70% of them fall under Ca^{2+}, Na^+, and Mg^{2+} water types, respectively. In the anion triangle, around 70.37% of the samples fall under HCO_3^- water type, while 22.22% of them under Cl^- water type.

3.3.2. Classification based on specific ion concentration

Soltan (1998) classified the concentrations of Cl^-, SO_4^{2-}, and HCO_3^- ions in groundwater as (i) normal Cl^- (<15 meq/l), (ii) normal SO_4^{2-} (<6 meq/l), and (iii) normal HCO_3^- (2–7 meq/l). As such, while all groundwater samples show normal Cl^- and normal SO_4^{2-} concentrations (Table 2), in the case of HCO_3^-, 7.4% of the samples are below their normal concentration levels.

Base exchange indices (r_1): Base exchange indices (r_1) are used to study the dominant chemical constituent that determines the water facies, as shown in Eq. (2) (Soltan, 1998).

$$r_1 = \frac{Na^+ - Cl^-}{SO_4^{2-}} \tag{2}$$

where, Na^+, Cl^- and SO_4^{2-} concentrations are expressed in meq/l.

A value of $r_1 < 1$ indicates Na^+ - SO_4^{2-} water type, and $r_1 > 1$, Na^+-HCO_3^- water type. Based on this equation, most samples (59.26%) are Na^+- HCO_3^- water type, indicating ion exchange and silicate mineral dissolution as the key processes in the aquifers. The remaining 40.74% of the samples show Na^+- SO_4^{2-} type depicting reverse ion exchange processes (Table 2).

Meteoric genesis index (r_2): Soltan (1998) also used another index, called meteoric genesis index (r_2), to classify the water sources into two types, as follows (Eq. (3)).

$$r_2 = \frac{(Na^+ + K^+) - Cl^-}{SO_4^{2-}} \tag{3}$$

where, Na^+, K^+, Cl^- and SO_4^{2-} are the concentrations of the water samples in meq/l.

Meteoric water, in the context of this paper, refers to water that originates from precipitation, such as rain, which then contributes to the groundwater system. The water that recharges the groundwater affects the redox conditions in the aquifers. The value of $r_2 < 1$ indicates deep meteoric water percolation type, whereas that of $r_2 > 1$, shallow meteoric water percolation type. Under this classification, most samples (62.96%) in the study area are characterized as shallow meteoric water percolating type. The remaining 37.04% of the samples are classified as deep meteoric percolation water type (Table 2). Under natural conditions, chemical composition of groundwater changes from HCO_3^- type at shallower depth to Cl^- type as the depth increases due to small evapotranspiration losses (Brown et al., 1977). Therefore, many samples (G5, G16, G17, G18, G19, G22, G23, G24, G25, and G26) characterized by the deep meteoric water percolation type exhibit higher concentrations of Cl^- ions over strong acids (Na^+ and K^+) in the study area.

3.4. Index of Base Exchange (IBE)

Scholler (1965) developed two Chloroalkaline indices, *CAI-I* and *CAI-II*, to determine the magnitude of base exchange (IBE) processes occurring between the groundwater and the host aquifers (Eqs. 4 and 5, with concentrations of ions expressed in meq/l.).

$$CAI - I = \frac{Cl^- - (Na^+ + K^+)}{Cl^-} \tag{4}$$

$$CAI - II = \frac{Cl^- - (Na^+ + K^+)}{\left(HCO_3^- + CO_3^- + SO_4^{2-} + NO_3^-\right)} \tag{5}$$

These indices (*CAI-I* and *CAI-II*) assist in the assessment of the nature of ion exchange processes (cation exchange or reverse ion exchange) that occur between the recharging water and the aquifer material during the residence time of water in its flow path (Singh et al., 2020b). The negative and positive values of both *CAI-I* and *CAI-II* signal cation exchange and reverse ion exchange processes, respectively, in the aquifer system. In the standard ion/cation exchange process, when water passes through the aquifer in its flow path, ions in the water are attracted to the ions in the aquifer by displacing them. In the reverse ion exchange process, these ions are exchanged back from the aquifer into the solution, essentially reversing the standard ion exchange process. This process selectively removes chemicals from the water by swapping out ions at favorable exchangeable sites from the aquifer matrix. Therefore, the residence time of groundwater in the aquifer system is highly important (Balaji et al., 2017; Singh et al., 2020b).

When these two indices (*CAI-I* and *CAI-II*) give negative values, the sodium and potassium in the host rock replace the calcium and magnesium in the groundwater. This condition is known as cation exchange process (chloro-alkaline disequilibrium). On the contrary, when the two indices give positive values, sodium and potassium in groundwater exchange with the calcium and magnesium of the host rock/aquifer (base exchange or reverse ion exchange) to maintain chloro-alkaline equilibrium. Approximately 70.37% of the groundwater samples show negative *CAI-I* and *CAI-II* indices, indicating the cation exchange process ($Cl^- < Na^+ + K^+$), where host rocks are the primary sources of dissolved solids in water (Table 2). The remaining 29.63% of the samples exhibit positive values reflecting base exchange reaction or reverse ion exchange process ($Cl^- > Na^+ + K^+$) (Table 2). The general reactions of chloro-alkaline disequilibrium and base exchange reactions in the aquifer system are given below.

$$Na^+(K^+) - Clay + Ca^{2+}\left(Mg^{2+}\right)aq = 2Na^+(K^+)aq + Ca^{2+}\left(Mg^{2+}\right) - Clay - CX \tag{6}$$

Table 2
Groundwater characterization and ionic ratios of the analyzed parameters of the groundwater samples from the village Supebeda, Chhattisgarh State, India.

Sample nos.	Ca^{2+}/Mg^{2+}	Cl^-	SO_4^{2-}	HCO_3^-	*r1*	Water type	*r2*	Water type	IBE		$Ca^{2+}/(Ca^{2+}+Mg^{2+})$	$(Ca^{2+}+Mg^{2+})/TZ^+$	$Ca^{2+}/(Ca^{2+}+SO_4^{2-})$	$(Na^++K^+-Cl^-)/(Na^++K^+-Cl^-+Ca^{2+})$	Na^+/Cl^-	$Na^+/(Na^++Cl^-)$	$(Ca^{2+}+Mg^{2+})/(Na^++K^+)$	$(Na^++K^+)/TZ^+$
									CAI-I	CAI-II								
		meq/L																
G1	0.94	0.50	0.11	7.81	37.71	Na^+-HCO_3^-	37.84	SM	−8.47	−0.54	0.49	0.38	0.93	0.75	9.44	0.90	12.44	0.62
G2	0.56	0.40	0.21	7.10	14.03	Na^+-HCO_3^-	14.33	SM	−7.67	−0.42	0.36	0.55	0.87	0.67	8.51	0.89	6.99	0.45
G3	0.65	0.60	0.20	6.20	14.34	Na^+-HCO_3^-	14.92	SM	−5.01	−0.46	0.40	0.43	0.84	0.73	5.82	0.85	5.44	0.57
G4	1.89	0.20	0.10	5.51	32.15	Na^+-HCO_3^-	32.31	SM	−16.11	−0.57	0.65	0.40	0.94	0.68	17.03	0.94	14.99	0.60
G5	1.52	0.90	0.12	3.71	−1.59	Na^+-SO_4^{2-}	−1.30	DM	0.17	0.04	0.60	0.86	0.96	−0.06	*0.80*	0.44	23.13	0.14
G6	0.63	0.60	0.19	3.51	0.60	Na^+-SO_4^{2-}	1.11	SM	−0.35	−0.05	0.39	0.83	0.89	0.12	1.19	0.54	8.00	0.17
G7	1.64	0.50	0.20	2.20	1.57	Na^+-HCO_3^-	1.79	SM	−0.70	−0.13	0.62	0.71	0.87	0.21	1.61	0.62	6.64	0.29
G8	4.29	0.30	0.13	4.40	20.50	Na^+-HCO_3^-	20.64	SM	−8.82	−0.58	0.81	0.41	0.93	0.61	9.76	0.91	13.16	0.59
G9	3.46	0.30	0.17	5.10	11.15	Na^+-HCO_3^-	11.35	SM	−6.49	−0.37	0.78	0.58	0.93	0.45	7.38	0.88	13.87	0.42
G10	1.94	0.50	0.15	4.10	3.54	Na^+-HCO_3^-	3.69	SM	−1.12	−0.13	0.66	0.77	0.94	0.20	2.07	0.67	15.12	0.23
G11	1.48	0.30	0.14	3.39	6.61	Na^+-HCO_3^-	6.82	SM	−3.10	−0.21	0.60	0.72	0.93	0.33	4.01	0.80	13.81	0.28
G12	1.84	0.50	0.26	4.40	5.46	Na^+-HCO_3^-	5.54	SM	−2.85	−0.31	0.65	0.61	0.89	0.42	3.80	0.79	7.74	0.39
G13	2.22	0.70	0.29	4.10	2.80	Na^+-HCO_3^-	2.90	SM	−1.20	−0.19	0.69	0.67	0.88	0.28	2.16	0.68	7.54	0.33
G14	1.33	0.70	1.54	3.49	1.17	Na^+-HCO_3^-	1.19	SM	−2.60	−0.33	0.57	0.59	0.58	0.47	3.56	0.78	1.36	0.41
G15	1.95	1.70	0.12	7.81	29.55	Na^+-HCO_3^-	32.01	SM	−2.23	−0.44	0.66	0.43	0.96	0.58	3.06	0.75	22.73	0.57
G16	1.32	0.70	1.86	1.71	0.29	Na^+-SO_4^{2-}	*0.31*	DM	−0.82	−0.15	0.57	0.70	0.48	0.25	1.77	0.64	0.91	0.30
G17	2.83	11.51	2.19	6.81	−1.57	Na^+-SO_4^{2-}	−1.53	DM	0.29	0.31	0.74	0.62	0.82	−0.52	0.70	0.41	4.46	0.38
G18	1.93	10.71	0.12	8.51	−23.39	Na^+-SO_4^{2-}	−22.97	DM	0.26	0.28	0.66	0.62	0.99	−0.49	0.74	0.42	69.49	0.38
G19	2.15	2.70	0.19	4.20	−5.65	Na^+-SO_4^{2-}	−5.25	DM	0.37	0.17	0.68	0.81	0.96	−0.24	0.60	0.38	26.89	0.19
G20	3.37	0.40	1.03	4.10	3.45	Na^+-HCO_3^-	3.48	SM	−8.92	−0.68	0.77	0.25	0.49	0.78	9.84	0.91	0.97	0.75
G21	2.47	0.30	0.64	4.90	3.55	Na^+-HCO_3^-	3.59	SM	−7.68	−0.40	0.71	0.54	0.77	0.51	8.58	0.90	3.41	0.46
G22	1.52	2.70	0.61	4.51	−0.23	Na^+-SO_4^{2-}	−0.15	DM	0.03	0.01	0.60	0.74	0.88	−0.02	0.95	0.49	7.37	0.26
G23	2.07	2.20	1.77	1.39	−0.68	Na^+-SO_4^{2-}	−0.66	DM	0.53	0.27	0.67	0.85	0.70	−0.40	0.46	0.31	2.31	0.15
G24	4.55	1.80	0.99	6.20	0.67	Na^+-SO_4^{2-}	0.75	DM	−0.41	−0.10	0.82	0.72	0.85	0.12	1.37	0.58	5.47	0.28

(*continued on next page*)

Table 2 (*continued*)

Sample nos.	Ca^{2+}/Mg^{2+}	Cl^-	SO_4^{2-}	HCO_3^-	*r1*	Water type	*r2*	Water type	IBE		$Ca^{2+}/(Ca^{2+}+Mg^{2+})$	$(Ca^{2+}+Mg^{2+})/TZ^+$	$Ca^{2+}/(Ca^{2+}+SO_4^{2-})$	$(Na^++K^+-Cl^-)/(Na^++K^++Cl^-+Ca^{2+})$	Na^+/Cl^-	$Na^+/(Na^++Cl^-)$	$(Ca^{2+}+Mg^{2+})/(Na^++K^+)$	$(Na^++K^+)/TZ^+$
									CAI-I	CAI-II								
G25	2.46	7.81	1.34	5.40	−4.05	Na^+-SO_4^{2-}	−4.00	DM	0.69	0.61	0.71	0.86	0.89	−1.01	0.31	0.23	7.97	0.14
G26	2.10	4.51	0.50	5.51	−2.12	Na^+-SO_4^{2-}	−1.96	DM	0.22	0.13	0.68	0.68	0.91	−0.23	0.76	0.43	10.35	0.32
G27	4.95	2.10	1.12	5.51	1.00	Na^+-HCO_3^-	1.06	SM	−0.57	−0.15	0.83	0.64	0.81	0.20	1.53	0.61	4.35	0.36
Mean	2.15	2.08	0.60	4.87	5.59		5.84		−3.06	−0.16	0.64	0.63	0.85	0.20	3.99	0.66	11.74	0.37
Min.	0.56	0.20	0.10	1.39	−23.39		−22.97		−16.11	−0.68	0.36	0.25	0.48	−1.01	0.31	0.23	0.91	0.14
Max.	4.97	11.51	2.19	8.51	37.71		37.84		0.69	0.32	0.83	0.86	0.99	0.78	17.03	0.94	69.49	0.75

Abbreviations: *r1* = Base Exchange Index. *r2* = Meteoric Genesis Index. IBE = Index of Base Exchange. *CAI* = Chloroalkaline Index (*CAI-I* and *CAI-II*: Bold *CAI-I* and *CAI-II* values indicate reverse ion exchange processes. Italics *CAI-I* and *CAI-II* values indicate cation exchange conditions). SM = Shallow Meteoric. DM = Deep Meteoric.

$$Na^+(K^+)aq + Ca^{2+}\left(Mg^{2+}\right) - Clay = 2Na^+(K^+) - Clay + Ca^{2+}\left(Mg^{2+}\right)aq - RX \quad (7)$$

Permutolites are clay minerals which absorb and exchange their cations with the cations present in water. Clay minerals like kaolinite, illite, chlorite, and halloysite have poor ionic exchange capacity because the exchangeable ions are held at their edges (Thilagavathi et al., 2012). On the other hand, montmorillonite, and vermiculite minerals have a greater number of exchangeable ions that are held on the surface resulting in a higher ionic exchange capacity when in contact with water (Thilagavathi et al., 2012).

3.5. Source apportionment of chemical signatures

Numerous indirect and direct processes occur between the host rocks and groundwater. The interionic ratios of different chemical parameters can be graphically represented in order to identify various geochemical signatures for source apportionment, such as for identifying the roles of geogenic/anthropogenic inputs, salinization, ion exchange processes, etc.

3.5.1. Direct and indirect processes

The bivariate plot between [(Ca^{2+}+Mg^{2+}) - (HCO_3^- + SO_4^{2-})] vs. [(Na^++K^+)-Cl^-] is prepared to verify the cation exchange process occurring in groundwater (Fig. 2a). McLean et al. (2000) conclude that when the entire data plot clusters around the origin, cation exchange is not prominent in the groundwater system. On the other hand, when the bivariate plot follows a linear slope of −1, cation exchange is the key geochemical process controlling the hydrochemistry of groundwater. In the study area, the groundwater samples plot along the slope of −1 ($y = -1.316x + 0.684$; $R^2 = 0.97$), exhibiting ion exchange between Ca^{2+}, Mg^{2+}, and Na^+, K^+ in the aquifer system (Fig. 2a). Further, 62.93% of the samples fall in quadrant B indicating the cation exchange process (Ca^{2+}, Mg^{2+} < Na^+) and 22.22% of the samples lie in quadrant A showing a reverse ion exchange process (Ca^{2+}, Mg^{2+} > Na^+). The remaining 11.11% of the samples cluster around the origin of the bivariate plot depicting dissolution of minerals, and only 3.70% of the samples scatter away from the slope line due to other factors (Bahir et al., 2018; Marghade, 2020).

The plot (Na^++K^+) vs. (Ca^{2+}+Mg^{2+}) enables the prediction of chemical processes between the alkaline and alkali cations in groundwater. A weak R^2 value (i.e., R^2 = 0.23) reveals multisource of geochemical processes generating these ions (Fig. 2b). Most of the samples (77.78%) fall below the equiline 1:1 displaying cation exchange activity, and the remaining 22.22% of the samples plot above the equiline showing reverse ion exchange process. The presence of clay material reduces the permeability potential in the region, enabling the reverse ion exchange process by releasing Ca^{2+} and Mg^{2+} in percolating water and absorbing Na^+ and K^+ in the clay matrix (Howard and Lloyd, 1983).

3.5.2. Minerals inducing ion exchange

The scatter plot of Ca^{2+} + Mg^{2+} vs. HCO_3^- + SO_4^{2-} is an important geochemical signature to identify the exchange process in the aquifer system (Singh et al., 2020b; Rajkumar et al., 2023). Fig. 2c shows that 66.66% of the samples plot below the 1:1 equiline, depicting silicate weathering as the primary process of ion exchange. Thus, increased concentrations of HCO_3^- have been balanced by alkalis (Na^+ + K^+) in groundwater. Around 29.63% of the groundwater samples cluster above the 1:1 line, exhibiting carbonate weathering as the leading cause of the reverse ion exchange process (Okiongbo and Douglas, 2015). Nearly 3.70% of the samples fall on the equiline (1:1), reflecting the influence of calcite, gypsum, and dolomite dissolution in groundwater (Singh et al., 2017). Similarly, the interionic plot between Na^+ vs. Ca^{2+} further supports the role of ion exchange and dissolution of silicate and

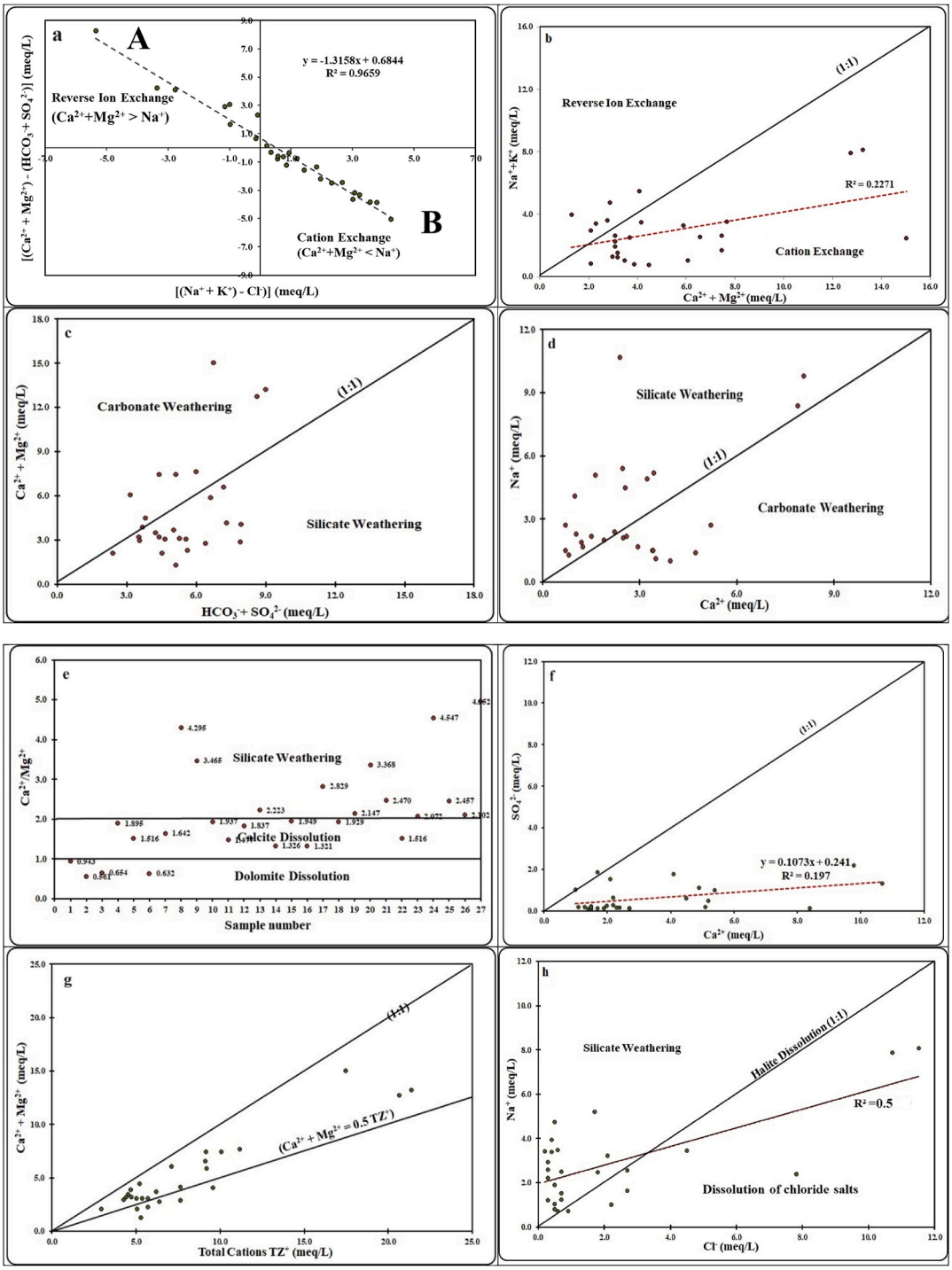

Fig. 2. Interionic relationship between major ions in groundwater in the village Supebeda, Gariabandh District, Chhattisgarh State, India. (a) $[(Ca^{2+}+Mg^{2+})-(HCO_3^- + SO_4^{2-})]$ vs $[(Na^+ + K^+)-Cl^-]$, (b) $(Na^+ + K^+)$ vs $(Ca^{2+}+Mg^{2+})$, (c) $Ca^{2+} + Mg^{2+}$ vs $HCO_3^- + SO_4^{2-}$, (d) Na^+ vs Ca^{2+}, (e) Ca^{2+}/Mg^{2+}, (f) Ca^{2+} vs SO_4^{2-}, (g) $Ca^{2+} + Mg^{2+}$ vs Total Cations (TZ^+), (h) Na^+ vs Cl^-, (i) Na^+/Cl^- vs EC, (j) $Na^+ + K^+$ vs $SO_4^{2-} + Cl^-$, and (k) $Na^+ + K^+$ vs TZ^+.

carbonate minerals in the study area (Fig. 2d).

3.5.3. *Weathering and dissolution*

The Ca^{2+}/Mg^{2+} ratio is plotted to ascertain the probable contributing mineral sources of Ca^{2+} and Mg^{2+} ions in groundwater. Around 14.81% and 44.44% of the samples have Ca^{2+}/Mg^{2+} ratios of <1 and >2, respectively, indicating an undersaturated state of dolomite dissolution and silicate weathering (Singh et al., 2020a; Zhou et al., 2020) (Fig. 2e). The remaining 40.74% of the samples fall within 1 and 2 revealing the undersaturated state of calcite dissolution in groundwater. The general chemical reactions of dolomite and calcite in the groundwater are expressed in Eqs. 8 and 9 (Zhang et al., 2020; Rajkumar et al., 2023).

$$\underset{\text{(Dolomite)}}{CaMg(CO_3)_2} + 2CO_2 + 2H_2O \rightarrow Ca^{2+} + Mg^{2+} + 4HCO_3^- \quad (8)$$

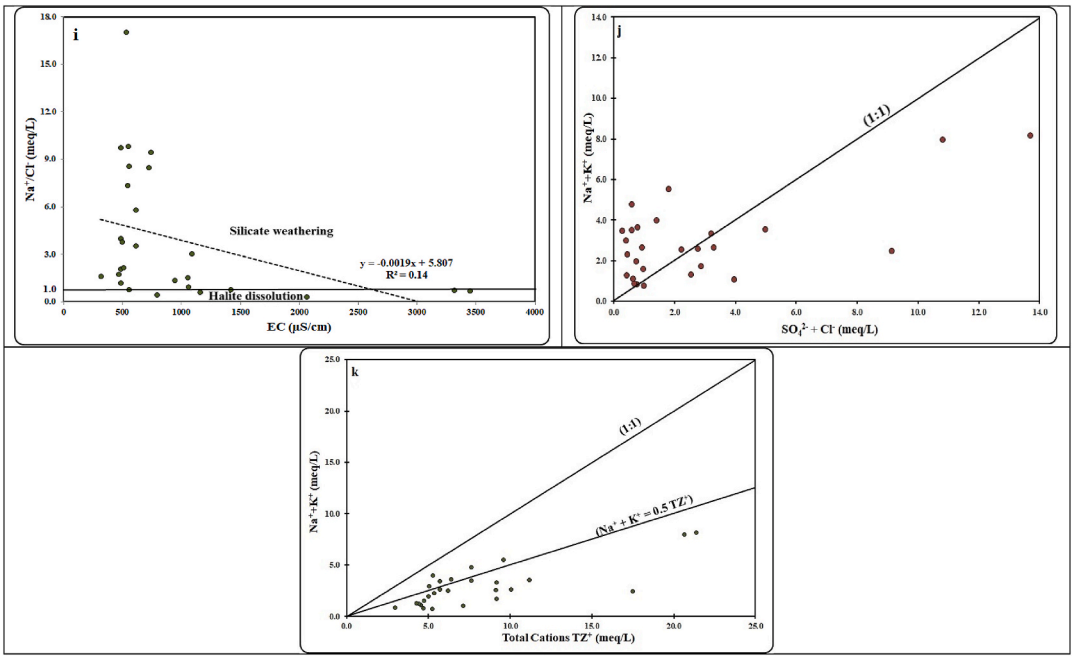

Fig. 2. (*continued*).

$$\underset{\text{(Calcite)}}{CaCO_3} + H_2O + CO_2 \rightarrow Ca^{2+} + 2HCO_3^- \quad (9)$$

The values of $[Ca^{2+}/(Ca^{2+}+Mg^{2+})]$ ratio vary from 0.36 to 0.83 (Table 2). About 14.81% of the samples have $[Ca^{2+}/(Ca^{2+}+Mg^{2+})]$ ratio of <0.5 confirming the precipitation of calcite and dissolution of dolomite, thus reflecting a higher Mg^{2+} concentration than Ca^{2+} (Herojeet et al., 2016). The remaining samples (85.19%) are solely influenced by the weathering of calcsilicate minerals in the aquifer system as the ratio of $[Ca^{2+}/(Ca^{2+}+Mg^{2+})]$ is > 0.5. The metamorphic rocks at Supebeda are rich in anorthite ($CaAl_2Si_2O_8$), amphibole $[Ca_2Mg_5Si_8O_{22}(OH)_2]$, hornblende $[(Ca,Na)_2(Mg,FeAl)_5(Al,Si)_8O_{22}(OH)_2]$, and biotite $[K(Mg,Fe)_2AlSi_3O_3(F,OH)_2]$ minerals. Therefore, carbonate, calcsilicate, and silicate minerals in host rocks influence Ca^{2+} and Mg^{2+} concentrations in groundwater due to rock-water interactions (Eqs. 8–12).

$$\underset{\text{(Anhydrite and dolomite)}}{CaSO_4 + CaMgCO_3 + 6H^+} \leftrightarrow CaCO_3 + Ca^{2+} + Mg^{2+} + SO_4^{2-} + H_2CO_3 \quad (10)$$

$$\underset{\text{(Anorthite)}}{CaAl_2Si_2O_8} + 2H^+ + H_2O \rightarrow Al_2Si_2O_5(OH)_4 + Ca^{2+} \quad (11)$$

$$\underset{\text{(Amphibole)}}{Ca_2Mg_5Si_8O_{22}(OH)_2} + 14CO_2 + 22H_2O \rightarrow 2Ca^{2+} + 5Mg^{2+} + 14HCO_3^- + 8Si(OH)_4 \quad (12)$$

Further, the dissolution of gypsum mineral contributes to the Ca^{2+} and SO_4^{2-} ions in water, as given in Eq. (13). But Fig. 2f shows that most of the samples (92.6%) plot below the equiline (1:1), indicating the role of gypsum ($CaSO_4.2H_2O$) dissolution as insignificant in the study area. The remaining samples (7.4%) fall along the equiline depicting the dissolution of anhydrite ($CaSO_4$) mineral in groundwater (Purushothaman et al., 2014; Kumari et al., 2018). The ionic ratio $[Ca^{2+}/(Ca^{2+}+SO_4^{2-})]$ varies from 0.48 to 0.99 (Table 2) with 92.6% of the samples giving a value of >0.5, divulging that carbonate, calc-silicate, and silicate minerals contribute to the Ca^{2+} concentration in groundwater. Hence, the weak positive correlation between Ca^{2+} vs. SO_4^{2-} ($r^2 = 0.197$) supports diverse sources of Ca^{2+} and SO_4^{2-} ions in the study area (Fig. 2f).

$$\underset{\text{(Gypsum)}}{CaSO_4.2H_2O} \rightarrow Ca^{2+} + SO_4^{2-} + 2H_2O \quad (13)$$

3.5.4. Mixed factors (geogenic and anthropogenic)

The $Ca^{2+} + Mg^{2+}$ vs. Total Cations (TZ^+) (ratio = 0.63, Table 2) bivariate plot (Fig. 2g) shows 77.78% of the samples plotting between the 1:1 and $Ca^{2+}+Mg^{2+} = 0.5\ TZ^+$ lines. Thus, the total cation concentrations in the groundwater samples show a significant contribution of the alkaline metals. The sources of Ca^{2+} and Mg^{2+} in the groundwater are derived from the weathering of carbonate (calcite, dolomite), anhydrite, gypsum, calc-silicate (anorthite, plagioclase, amphiboles), and ferromagnesian minerals (hornblende, biotite) in the metamorphic rocks (Herojeet et al., 2023; Neogi et al., 2017). The remaining 22.22% of the groundwater samples scattered below the $Ca^{2+}+Mg^{2+} = 0.5\ TZ^+$ line depict silicate weathering and anthropogenic inputs, namely chemical fertilizers, seepage of domestic sewerage etc., contributing to the increasing concentrations of alkalis (Mahaqi et al., 2018; Singh et al., 2020a).

The groundwater salinity in the arid and semi-arid regions can be illustrated by a scatter plot between Na^+ vs. Cl^- (Fig. 2h) (Gaofeng et al., 2010; Singh et al., 2020b). This figure shows that about 66.66% of the samples are distributed above the equiline (1:1), confirming silicate (albite) weathering and cation exchange processes enriching the Na^+ concentration in groundwater. Only 7.40% of the samples fall on the equiline (1:1), indicating that halite dissolution does not significantly affect the concentrations of Na^+ and Cl^- in the aquifer system, as shown in Eq. (14). Further, the remaining samples (22.22%) fall below the $y = x$ line, suggesting the impact of anthropogenic inputs and dissolution of Cl^- salts (Rajkumar et al., 2023). It is important to note here that the Piper diagram indicates that 22.22% of the samples are Cl^- dominant water type, thus confirming the anthropogenic influence on groundwater (Fig. S3). The moderately positive regression line value ($R^2 = 0.5$) between Na^+ vs. Cl^- in Fig. 2h attributes their origin to the geogenic and anthropogenic sources.

$$\underset{\text{(Halite)}}{NaCl} \rightarrow Na^+ + Cl^- \quad (14)$$

Further, the scatter plot of Na^+/Cl^- vs. EC (Fig. 2i) supports that the

dissolution of silicate (albite) and halite minerals, ion exchange, and anthropogenic factors increase the Cl^- concentration and its mobility relative to Na^+ in groundwater (He et al., 2019). The inclined trendline ($y = -0.0019x$) and weak correlation score ($R^2 = 0.14$) of Na^+/Cl^- vs. EC indicate that evaporation is not the dominant factor influencing groundwater chemistry (Subramani et al., 2010). This observation is supported by the Gibbs diagram (Fig. S4a), and end member plots (Fig. S4 (b, c)).

Moreover, the ratio of $[(Na^+ + K^+ - Cl^-)/(Na^+ + K^+ - Cl^- + Ca^{2+})]$ ranging between (−1.01) and 0.78 (Table 2), with ~62.9% of the samples showing an ionic ratio higher than >0.2, further subtends the possibility of plagioclase weathering (Marghade, 2020) (Eqs. 15 and 16). The remaining samples (37.1%) divulge halite dissolution and base exchange processes in groundwater. The ratios of $[Na^+/(Na^+ + Cl^-)]$ and Na^+/Cl^- range from 0.31 to 17.03 and 0.23–0.94, respectively (Table 2). About 70.37% of the samples have higher values of $[Na^+/(Na^+ + Cl^-)]$ >0.5 and Na^+/Cl^- >1, indicating that the dissolution of silicate (albite) is not the only source of Na^+ concentration; other factors, such as halite dissolution, ion exchange, and anthropogenic inputs also contribute to the generation of Na^+ ions in groundwater (Marghade, 2020; Rajkumar et al., 2023). The remaining 29.63% of the samples show $[Na^+/(Na^+ + Cl^-)]$ and Na^+/Cl^- values of <0.5 and < 1, respectively, reflecting halite dissolution contributing to the Na^+ and Cl^- ions at Supebeda.

$$\underset{\text{(Albite)}}{2NaAlSi_3O_8} + 2CO_2 + 11H_2O \rightarrow Al_2Si_2O_5(OH)_4 + 4H_4SiO_4 + 2Na^+ + 2HCO_3^- \quad (15)$$

$$\underset{\text{(K - feldspar)}}{KAlSi_3O_8} + CO_2 + 3H_2O \rightarrow Al_2Si_2O_5(OH)_4 + K^+ + 2SiO_2 + HCO_3^- \quad (16)$$

Fig. 2j shows that the plot of $Na^+ + K^+$ vs. $SO_4^{2-} + Cl^-$ clusters close to the theoretical line (1:1) with a moderate positive trendline value of $R^2 = 0.42$. This reflects the common sources of these ions from the dissolution of soil salts and anthropogenic activities (Panda et al., 2018; Datta and Tyagi, 1996). The bivariate plot of $Na^+ + K^+$ vs. TZ^+ (Fig. 2k) depicts that 22.22% of the samples grouped between the 1:1 and $Na^+ + K^+ = 0.5TZ^+$ lines imply the influence of silicate weathering, ion exchange and the anthropogenic inputs on soil contributing to Na^+ and K^+ concentrations in groundwater (Stallard and Edmond, 1983). The relatively high average ratio of $(Ca^{2+} + Mg^{2+})/(Na^+ + K^+)$, i.e., 2.33, and the low average ratio of $Na^+ + K^+/TZ^+$ (0.37) (Table 2) indicate the dominance of alkaline earth metals over alkalis. This is supported by 77.78% of the samples plotting below the $Na^+ + K^+ = 0.5TZ^+$ trend line (Fig. 2k). The dissolution of calcite, dolomite, anorthite and amphibole, and ion exchange processes have elevated the concentrations of alkaline earth metals (Ca^{2+} and Mg^{2+}) in the groundwater of the Supebeda region.

3.6. Linking hydrochemistry with CKDu

The order of predominant cations and anions in the groundwater samples in Supebeda region is as follows: $Ca^{2+} > Na^+ > Mg^{2+} > K^+$ (cations) and $HCO_3^- > Cl^- > NO_3^- > SO_4^{2-} > F^-$ (anions) (Fig. S5). As discussed before, 33.33% of the groundwater samples show Ca^{2+} concentration above its acceptable limit of 75 mg/L (BIS, 2020), while in case of Mg^{2+}, about 19% of the samples exceed its acceptable limit of 30 mg/L. These elevated concentrations influence the total hardness (TH) in groundwater chemistry with 44.44% of the samples above the BIS (2020) acceptable limit of 200 mg/L that include 11.11% of the samples exceeding its permissible limit of 600 mg/L. The concentrations of alkali metals (Na^+ and K^+) are within their respective guideline values (WHO, 2022), however. Further, the results of Piper diagram (Fig. S3) reveal that Ca^{2+}-Mg^{2+}-HCO_3^- (55.56%, showing temporary hardness) and Ca^{2+}-Mg^{2+}-Cl^--SO_4^{2-} (29.63%, showing permanent hardness) are the dominant facies followed by that of alkali carbonate Na^+-K^+-HCO_3^- in 14.81% of the samples. Among the anions, F^- and NO_3^-, with all their negative health implications (WHO, 2022; Herojeet et al., 2023), are the key violator parameters. About 41% of the samples exhibit F^- concentrations above the BIS (2020) acceptable limit of 1.0 mg/L including 26% of the samples exceeding the permissible limit of 1.5 mg/L. In case of NO_3^-, 37% of the samples exceed their guideline value of 45 mg/L (BIS, 2020; WHO, 2022). Other parameters, namely HCO_3^-, and Cl^- exceed their acceptable limits by 3.7%, and 11.11%, respectively (Table 1).

Among all chemical elements in the Periodic Table, fluorine (F), in the form of fluoride (F^-) ions, has the strongest tendency to attract electrons with its electronegativity value varying between 3.78 and 24.8 in various scales (Sproul, 2020). The disease CKDu is found to be associated with higher concentrations of F^- ions and total hardness in groundwater (Liyanage et al., 2022; Chandrajith et al., 2024; Rajkumar et al., 2025a). There is a reciprocal relationship between the F^- concentration in the blood serum and its content in urine discharges (Exner (2001). This synergy has been exemplified in CKDu patients at Supebeda as well (Chowdhary et al., 2020). The ionic activity ratios of Na^+/Ca^{2+} and Na^+/Mg^{2+} signal hydrochemical conditions affecting water hardness and fluoride enrichment. About 44% and 89% of the samples have Na^+/Ca^{2+} >1 and Na^+/Mg^{2+} >1, respectively, demonstrating favorable water chemistry for dissolution F^- ions in groundwater from fluoride-bearing minerals, such as fluorite, amphiboles, biotite, hornblende granite gneiss, etc., in rocks (Herojeet et al., 2023). The positive trendline between Na^+ vs. F^- ($R^2 = 0.2$, Fig. S6) divulges that the proportional increase of F^- concentration with the Na^+ ions in groundwater under alkaline pH condition (mean = 7.9; Table 1) favors dissolution of fluoride-bearing minerals (Saxena and Ahmed, 2003). The remaining 55% and 11% of the samples have Na^+/Ca^{2+} <1 and Na^+/Mg^{2+} <1, respectively, depicting the roles of Ca^{2+} and Mg^{2+} ions in influencing the water hardness. Further, the bivariate plots of Na^+/Ca^{2+} vs. F^- and Na^+/Mg^{2+} vs. F^- regress positively with their R^2 value as 0.4 in both figures (Figs. S7 and S8). Under these conditions, this discussion infers that excess F^- content has synergic relationship with higher Ca^{2+} and Na^+ ions and to a lesser extent with Mg^{2+} concentration in groundwater.

Therefore, fluoride being the uppermost electronegative element easily forms stable metal-fluoride complexes with Ca^{2+}, Mg^{2+}, and Na^{2+}, causing tubular dysfunction, protein denature of glomerular basement membrane, collagen breakdown, and finally chronic renal failure (Veron et al., 1993; Yiamouyiannis, 1983; Santoyo-Sanchez et al., 2013; Dharma-Wardana, 2018; Dharmaratne, 2019; Johnston and Strobel, 2020; Prša et al., 2020). The formation of such metal-complexes creates ion-ion effect causing 'Hofmeister phenomena' (Hofmeister, 1888), thereby altering the solubility and precipitation of compounds in the tubular areas of human kidneys. The increased accumulation of Hofmeister ions in the kidney depletes the water molecules due to change in the osmotic activity and denaturation of protein (Agalakova and Gusev, 2012; Kang et al., 2020). Dharma-Wardana et al. (2015) rank the ions in the 'Hofmeister series' as $K^+ > Na^+ > Mg^{2+} > Ca^{2+}$ for cations and $F^- > SO_4^{2-} > HCO_3^- > Cl^- > NO_3^-$ for anions by their capacity to denature proteins. Thus, it is hypothesized that the increased ionic activities due to elevated concentrations of F^-, Ca^{2+}, and Na^+ ions in groundwater through oral ingestion by humans as drinking water agravate the Hofmeister phenomena disrupting the primary functions of the kidneys, especially in its tubular areas, inviting a myriad of renal problems eventually causing its complete failure.

4. Conclusions

The appraisal of analytical results from the 27 groundwater samples with respect to BIS (2020) and WHO (2022) guidelines around the village Supebeda helps identify the violator parameters, such as TH,

Ca^{2+}, Mg^{2+}, Cl^{-}, NO_3^{-} and F^{-}, as well as their sources. The water classes by CWQI signify that ~52% of the samples are potable, and ~37% may be considered for drinking after adequate treatment. The remaining 11% of the samples are unfit for drinking and domestic needs but are still fit for irrigation and industrial purposes. A quarter of the samples have F^{-} as the single violator parameter where groundwater could be used for drinking after proper onsite treatment. In terms of geochemistry, several appraisal parameters, such as hydrochemical interpolations and inter-ionic relationships, have been applied to enable extraction of the dominant hidden features of the geochemical signatures and their sources that influence the chemical constituents of groundwater. Chemical concentrations of about 88% of the groundwater samples are attributed to rock-water interactions (weathering and dissolution), and the rest 12% to evaporation. About 78% of the samples are unaffected by salinity, while about 22% are slightly affected by salinity. These 22% of the samples are Cl^{-} water type influenced by the dissolution of Cl^{-} salts, and anthropogenic inputs. The positive correlation between Na^{+} and Cl^{-} attributes their origin to the geogenic and anthropogenic sources. Further, the strong correlation between Cl^{-} and NO_3^{-} reflects the effect of human-induced contamination. While the excess F^{-} ions are due to weathering and dissolution of fluoride-bearing minerals, cation exchange is the controlling factor for the concentrations of the alkalis and alkaline elements. The bivariate plot of [$(Ca^{2+}+Mg^{2+})$ - $(HCO_3^{-} + SO_4^{2-})$] vs. [$(Na^{+}+K^{+})$-Cl-], along with $(Na^{+}+K^{+})$ vs. $(Ca^{2+}+Mg^{2+})$, reveals that cation exchange is the dominant regulating process between the alkaline and alkali cations in groundwater. It is envisaged that the combined effects of Ca^{+} and Mg^{2+} ions controlling the total hardness, a higher Na^{+}/Ca^{2+} ratio, and increased F^{-} concentration are possibly the inducing factors for CKDu in the Supebeda region.

The present work is based on one-time sampling of the 27 groundwater samples collected from strategic locations in Supebeda area. More intensive samplings covering lateral, vertical and seasonal variations of the violator parameters are required for a better understanding of the etiology of CKDu. Moreover, the hydrochemistry of this CKDu-infected area should be compared with that of non-CKDu areas with similar geological and climatological conditions to enhance the value of such research. Last but not the least, scientists must listen to the people's perspectives on CKDu before recommending preventive measures for its eradication.

CRediT authorship contribution statement

Herojeet Rajkumar: Writing – original draft, Visualization, Validation, Software, Formal analysis, Data curation, Conceptualization. **Pradeep K. Naik:** Writing – review & editing, Visualization, Validation, Supervision, Resources, Project administration, Formal analysis, Conceptualization. **Rakesh K. Dewangan:** Project administration, Methodology, Investigation, Formal analysis. **Janak R. Verma:** Software, Investigation, Formal analysis, Data curation. **Prabir K. Naik:** Resources, Project administration, Investigation.

Declaration of competing interest

There is no conflict of interest.

Appendix A. Supplementary data

Supplementary data to this article can be found online at https://doi.org/10.1016/j.chemosphere.2025.144272.

Data availability

Data will be made available on request.

References

Agalakova, N.I., Gusev, G.P., 2012. Molecular mechanisms of cytotoxicity and apoptosis induced by inorganic fluoride. Int. Sch. Res. Not. 2012 (1), 403835.

Anupama, Y.J., Sankarasubbaiyan, S., Taduri, G., 2020. Chronic kidney disease of unknown etiology: case definition for India–a perspective. Indian J. Nephrol. 30 (4), 236–240. https://doi.org/10.4103/ijn.IJN_327_18.

APHA (American Public Health Association), 2005. Standard Methods for the Examination of Water and Wastewater, twenty-first ed. American Public Health Association, Washington, DC.

Awaleh, M.O., Boschetti, T., Ahmed, M.M., Dabar, O.A., Robleh, M.A., Waberi, M.M., Ibrahim, N.H., Dirieh, E.S., 2024. Spatial distribution, geochemical processes of high-content fluoride and nitrate groundwater, and an associated probabilistic human health risk appraisal in the Republic of Djibouti. Sci. Total Environ. 927, 171968. https://doi.org/10.1016/j.scitotenv.2024.171968.

Bahir, M., Ouazar, D., Ouhamdouch, S., 2018. Characterization of mechanisms and processes controlling groundwater salinization in coastal semi-arid area using hydrochemical and isotopic investigations (Essaouira basin, Morocco). Environ. Sci. Pollut. Res. 25, 24992–25004. https://doi.org/10.1007/s11356-018-2543-8.

Balaji, E., Nagaraju, A., Sreedhar, Y., Thejaswi, A., Sharifi, Z., 2017. Hydrochemical characterization of groundwater in around Tirupati area, Chittoor Dist., Andhra Pradesh, South India. Appl. Water Sci. 7, 1203–1212. https://doi.org/10.1007/s13201-016-0448-6.

BIS (Bureau of Indian Standards), 2020. Product manual for drinking water according to IS 10500: 2012. New Delhi. https://www.bis.gov.in/wp-content/uploads/2020/10/PM-IS-10500.pdf.

Bradley, M., Land, D., Thompson, D.A., Cwiertny, D.M., 2024. A critical review of a hidden epidemic: examining the occupational and environmental risk factors of chronic kidney disease of unknown etiology (CKDu). Environ. Sci.: Adv. https://doi.org/10.1039/D4VA00304G.

Campese, V.M., 2017. Con: mesoamerican nephropathy: is the problem dehydration or rehydration? Nephrol. Dial. Transplant. 32 (4), 603–606.

CAWST (Centre for Affordable Water and Sanitation Technology), 2009. Introduction to Drinking Water Quality Testing. CAWST, Calgary.

CDC (Centers for Disease Control and Prevention), 2020. Drinking Water Standards and Regulations. CDC, Atlanta.

CGWB (Central Ground Water Board), 2001. Basic Data Report of Exploratory Drilling at Deobhog in Raipur District, Madhya Pradesh. North Central Chhattisgarh Region, Raipur, CGWB, Govt. of India.

CGWB (Central Ground Water Board), 2022. Hydrogeology of Chhattisgarh. North Central Chhattisgarh Region, Raipur, CGWB, Govt. of India.

CGWB (Central Ground Water Board), 2023. Aquifer mapping and groundwater management plan of Gariyaband district, Chhattisgarh, North central Chhattisgarh region. Raipur, CGWB, Govt. of India.

Chandrajith, R., Nanayakkara, N., Zwiener, C., Daniel, C., Amann, K., Barth, J.A., 2024. Geochemical characteristics of groundwater consumed by patients with chronic kidney disease with unknown aetiology in the crystalline dry zone Terrain of Sri Lanka. Expo. Health 16 (1), 183–195. https://doi.org/10.1007/s12403-023-00547-y.

Chowdhary, P., Rathore, V., Jain, K., et al., 2020. CKD of unknown origin in Supebeda, Chhattisgarh, India. Kidney Int Rep 6, 210.

Das, R., Rao, N.S., Sahoo, H.K., Sakram, G., 2023. Nitrate contamination in groundwater and its health implications in a semi-urban region of Titrol block, Jagatsinghpur district, Odisha, India. Phys. Chem. Earth 132, 103424. https://doi.org/10.1016/j.pce.2023.103424. Parts A/B/C.

Datta, P.S., Tyagi, S.K., 1996. Major ion chemistry of groundwater in Delhi area: chemical weathering processes and groundwater flow regime. J. Geol. Soc. India 47, 179–188.

Dewangan, R., Verma, J.R., 2022. Groundwater Quality in Supebeda Area of Gariabandh District Chhattisgarh. (Central Groundwater Board, North Central Chhattisgarh Region Raipur. Department of Water resources, River Development and Ganga Rejuvenation, Ministry of Jal Shakti, Government of India, pp. 1–21.

Dharmaratne, R.W., 2019. Exploring the role of excess fluoride in chronic kidney disease: a review. Hum. Exp. Toxicol. 38 (3), 269–279.

Dharma-Wardana, M.W.C., 2018. Chronic kidney disease of unknown etiology and the effect of multiple-ion interactions. Environ. Geochem. Health 40, 705–719. https://doi.org/10.1007/s10653-017-0017-4.

Dharma-Wardana, M.W.C., Amarasiri, S.L., Dharmawardene, N., Panabokke, C.R., 2015. Chronic kidney disease of unknown aetiology and groundwater ionicity: study based on Sri Lanka. Environ. Geochem. Health 37 (2), 221–231. https://doi.org/10.1007/s10653-566014-9641-4.

Essue, B., Laba, T.L., Knaul, F., Chu, A., Minh, H., Nguyen, T.K.P., Jan, S., 2018. Economic burden of chronic Ill-health and injuries for households in low-and middle-income countries. Disease control priorities: improving health and reducing poverty. https://opus.lib.uts.edu.au/bitstream/10453/135163/1/TL_DCP3%20Volume%209_Ch%206.pdf.

Exner, F.B., 2001. A response to the American dental association's booklet fluoridation facts (Compiled by Anita Shattuck). In: Bennett, E. (Ed.), The Fluoride Debate. San Marcos: Health Way House, pp. 62–63 (Question 31).

Fiseha, T., Ekong, N.E., Osborne, N.J., 2024. Chronic kidney disease of unknown aetiology in Africa: a review of the literature. Nephrology 29 (4), 177–187.

Foreman, K.J., Marquez, N., Dolgert, A., Fukutaki, K., Fullman, N., McGaughey, M., Pletcher, M.A., Smith, A.E., Tang, K., Yuan, C.W., Brown, J.C., 2018. Forecasting life expectancy, years of life lost, and all-cause and cause-specific mortality for 250 causes of death: reference and alternative scenarios for 2016–40 for 195 countries and territories. Lancet 392, 2052–2090, 10159.

Galhotra, A., Rathore, V., Pal, R., Nayak, S., Ramasamy, S., Patel, S., Joshi, P., Nagarkar, N.M., Jha, V., 2023. Clinico-epidemiological profile of patients with chronic kidney diseases of unknown etiology: a hospital-based, cross-sectional study from Central India. Indian J. Nephrol. https://doi.org/10.4103/ijn.ijn_68_23.

Ganguli, A., 2016. Uddanam nephropathy/regional nephropathy in India: preliminary findings and a plea for further research. Am. J. Kidney Dis. 68 (3), 344–348.

Gaofeng, Z., Yonghong, S., Chunlin, H., et al., 2010. Hydrogeochemical processes in the groundwater environment of Heihe River Basin, northwest China. Environ. Earth Sci. 60, 139–153. https://doi.org/10.1007/s12665-009-0175-5.

GBD-CKDC (Chronic Kidney Disease Collaboration), 2020. Global, regional, and national burden of chronic kidney disease, 1990–2017: a systematic analysis for the Global Burden of Disease Study 2017. Lancet 395, 709–733, 10225.

Ghosh, R., Siddarth, M., Singh, N., Tyagi, V., Kare, P.K., Banerjee, B.D., Kalra, O.P., Tripathi, A.K., 2017. Organochlorine pesticide level in patients with chronic kidney disease of unknown etiology and its association with renal function. Environ. Health Prev. Med. 22, 1–8. https://doi.org/10.1186/s12199-017-0660-5.

Gupta, S., Bhattacharya, A., Raith, M., Nanda, J.K., 2000. Contrasting pressure–temperature–deformation history across a vestigial craton–mobile belt boundary: the western margin of the Eastern Ghats Belt at Deobhog, India. J. Metamorph. Geol. 18 (6), 683–697.

He, X., Wu, J., He, S., 2019. Hydrochemical characteristics and quality evaluation of groundwater in terms of health risks in Luohe aquifer in Wuqi County of the Chinese Loess Plateau, Northwest China. Hum. Ecol. Risk Assess. 25, 32–51. https://doi.org/10.1080/10807039.2018.1531693.

Herojeet, R., Dewangan, R.K., Naik, P.K., Verma, J.R., 2023. Probabilistic modelling is superior to deterministic approaches in the human health risk assessment: an example from a tribal stretch in central India. Sci. Rep. 13, 19351. https://doi.org/10.1038/s41598-023-45622-1.

Herojeet, R.K., Madhuri, S.R., Renu, L., Ranjna, G., 2016. Application of environmetrics statistical models and water quality index for groundwater quality characterization of alluvial aquifer of Nalagarh Valley, Himachal Pradesh, India. Sustain. Water Resour. Manag. 2, 39–53. https://doi.org/10.1007/s40899-015-0039-y.

Hettithanthri, O., Sandanayake, S., Magana-Arachchi, D., Wanigatunge, R., Rajapaksha, A.U., Zeng, X., Shi, Q., Guo, H., Vithanage, M., 2021. Risk factors for endemic chronic kidney disease of unknown etiology in Sri Lanka: retrospect of water security in the dry zone. Sci. Total Environ. 795, 148839.

Hofmeister, F., 1888. Zur Lehre von der Wirkung der Salze. Archiv f. experiment. Pathol. u. Pharmakol 24, 247–260. https://doi.org/10.1007/BF01918191.

Hounslow, A., 2018. Water Quality Data: Analysis and Interpretation. CRC Press).

Howard, K.W.F., Lloyd, J.W., 1983. Major ion characterization of coastal saline ground waters. Groundwater 21 (4), 429–437.

Imbulana, S., Oguma, K., 2021. Groundwater as a potential cause of Chronic Kidney Disease of unknown etiology (CKDu) in Sri Lanka: a review. J. Water Health 19 (3), 393–410.

John, O., et al., 2021. Chronic kidney disease of unknown etiology in India: what do we know and where we need to go. Kidney Int. Rep. 6 (11), 2743–2751. https://doi.org/10.1016/j.ekir.2021.07.031.

Johnston, N.R., Strobel, S.A., 2020. Principles of fluoride toxicity and the cellular response: a review. Arch. Toxicol. 94 (4), 1051–1069.

Jolly, A.M., Thomas, J., 2022. Chronic kidney disease of unknown etiology in India: a comparative study with Mesoamerican and Sri Lankan nephropathy. Environ. Sci. Pollut. Res. 29 (11), 15303–15317. https://doi.org/10.1007/s11356-021-16548-w.

Kang, B., Tang, H., Zhao, Z., Song, S., 2020. Hofmeister series: insights of ion specificity from amphiphilic assembly and interface property. ACS Omega 5 (12), 6229–6239. https://doi.org/10.1021/acsomega.0c00237.

Karunanidhi, D., Aravinthasamy, P., Subramani, T., Kumar, M., 2021. Human health risks associated with multipath exposure of groundwater nitrate and environmental friendly actions for quality improvement and sustainable management: a case study from Texvalley (Tiruppur region) of India. Chemosphere 265, 129083. https://doi.org/10.1016/j.chemosphere.2020.129083.

Khandare, A.L., Reddy, Y.S., Balakrishna, N., Rao, G.S., Gangadhar, T., Arlappa, N., 2015. Role of drinking water with high silica and strontium in chronic kidney disease: an exploratory community-based study in an Indian Village. Indian J. Community Health 27 (1), 95–102.

Kumari, R., Datta, P.S., Rao, M.S., et al., 2018. Anthropogenic perturbations induced groundwater vulnerability to pollution in the industrial Faridabad District, Haryana India. Environ. Earth Sci. 77, 187. https://doi.org/10.1007/s12665-018-7368-8.

Lal, K., Sehgal, M., Gupta, V., Sharma, A., John, O., Gummidi, B., Jha, V., Kumari, A., 2020. Assessment of groundwater quality of CKDu affected Uddanam region in Srikakulam district and across Andhra Pradesh, India. Groundw. Sustain. Dev. 11, 100432.

Levin, A., Okpechi, I.G., Caskey, F.J., Yang, C.W., Tonelli, M., Jha, V., 2023. Perspectives on early detection of chronic kidney disease: the facts, the questions, and a proposed framework for 2023 and beyond. Kidney Int. 103 (6), 1004–1008.

Liu, J., Peng, Y., Li, C., Gao, Z., Chen, S., 2021. An investigation into the hydrochemistry, quality and risk to human health of groundwater in the central region of Shandong Province, North China. J. Clean. Prod. 282, 125416. https://doi.org/10.1016/j.jclepro.2020.125416.

Liyanage, D.N.D., Diyabalanage, S., Dunuweera, S.P., Rajapakse, S., Rajapakse, R.M.G., Chandrajith, R., 2022. Significance of Mg-hardness and fluoride in drinking water on chronic kidney disease of unknown etiology in Monaragala, Sri Lanka. Environ. Res. 203, 111779. https://doi.org/10.1016/j.envres.2021.111779.

Mahaqi, A., Moheghi, M.M., Mehiqi, M., Moheghy, M.A., 2018. Hydrogeochemical characteristics and groundwater quality assessment for drinking and irrigation purposes in the Mazar-i-Sharif city, North Afghanistan. Appl. Water Sci. 8, 133. https://doi.org/10.1007/s13201-018-0768-9.

Maitra, A., Keesari, T., Roy, A., Gupta, S., 2021. Fluoride contamination in and around selected geothermal sites in Odisha, Eastern India: assessment of ionic relations, fluoride exposure and remediation. Environ. Sci. Pollut. Res. 28, 18553–21856. https://doi.org/10.1007/s11356-020-10948-0.

Marghade, D., 2020. Detailed geochemical assessment & indexing of shallow groundwater resources in metropolitan city of Nagpur (western Maharashtra, India) with potential health risk assessment of nitrate enriched groundwater for sustainable development. Geochemistry 80 (4), 125627. https://doi.org/10.1016/j.chemer.2020.125627.

Mascarenhas, S., Mutnuri, S., Ganguly, A., 2017. Deleterious role of trace elements–silica and lead in the development of chronic kidney disease. Chemosphere 177, 239–249. https://doi.org/10.1016/j.chemosphere.2017.02.155.

McLean, W., Jankowski, J., Levitt, N., 2000. Groundwater quality and sustainability in an alluvial aquifer, Australia. In: Sililo, O. (Ed.), Groundwater, Past Achievements and Future Chanllenges, pp. 567–573. Rotterdam, Balkenna.

Mogal, V., 2020. Study of incidence & clinical profile of chronic kidney disease of unknown etiology (Ckdu) in a tertiary referral center, Kidney Meet. In: 5th World Kidney Congress; Webinar- June 22-23, 2020.

Mohanty, N.K., Sahoo, K.C., Pati, S., Sahu, A.K., Mohanty, R., 2020. Prevalence of chronic kidney disease in cuttack district of Odisha, India. Int. J. Environ. Res. Publ. Health 17 (2), 456.

Mukherjee, I., Singh, U.K., 2022. Hydrogeochemical characterizations and quality evaluation of groundwater in the major river basins of a geologically and anthropogenically driven semi-arid tract of India. Sci. Total Environ. 805, 150323. https://doi.org/10.1016/j.scitotenv.2021.150323.

Nature, 2024. Time to sound the alarm about the hidden epidemic of kidney disease. Nature 628, 7–8. https://doi.org/10.1038/d41586-024-00961-5.

Nayak, S., Rehman, T., Patel, K., Dash, P., Alice, A., Kanungo, S., Palo, S.K., Pati, S., 2023. Factors associated with chronic kidney disease of unknown etiology (CKDu): a systematic review. Healthcare 11 (4), 551. https://doi.org/10.3390/healthcare11040551.

Neogi, B., Singh, A.K., Pathak, D.D., Chaturvedi, A., 2017. Hydrogeochemistry of coal mine water of North Karanpura coalfields, India: implication for solute acquisition processes, dissolved fluxes and water quality assessment. Environ. Earth Sci. 76, 1–17. https://doi.org/10.1007/s12665-017-6813-4.

Neogi, S., Das, N., 2000. Lithotectonic domains and metamorphic history of the boundary zone of the Eastern Ghats mobile belt and the Bastar craton, Deobhog area, Central India. Geol Surv India Spec. Publ. 57, 180–204.

Okiongbo, K.S., Douglas, R.K., 2015. Evaluation of major factors influencing the geochemistry of groundwater using graphical and multivariate statistical methods in Yengoa city, Southern Nigeria. Appl. Water Sci. 5, 27–37.

Panda, B., Chidambaram, S., Thilagavathi, R., Thivya, C., Ganesh, N., Devraj, N., 2018. Geochemical signatures of groundwater along mountain front and riparian zone of Courtallam, Tamil Nadu. Groundw. Sustain. Dev. 7, 372–386. https://doi.org/10.1016/j.gsd.2017.10.003.

Parameswaran, S., Rinu, P.K., Kar, S.S., Harichandrakumar, K.T., James, T.D., Priyamvada, P.S., Haridasan, S., Mohan, S., Radhakrishnan, J., 2020. A newly recognized endemic region of CKD of undetermined etiology (CKDu) in South India—"Tondaimandalam nephropathy". Kidney Int. Rep 5 (11), 2066–2073. https://doi.org/10.1016/j.ekir.2020.08.032.

Piper, A.M., 1944. A graphical procedure in the geochemical interpretation of water analysis. Am Geophys Union Trans 25, 914–928.

Priyadarshani, W.V.D., de Namor, A.F.D., Silva, S.R.P., 2023. Rising of a global silent killer: critical analysis of chronic kidney disease of uncertain aetiology (CKDu) worldwide and mitigation steps. Environ. Geochem. Health 45 (6), 2647–2662. https://doi.org/10.1007/s10653-022-01373-y.

Prša, P., Karademir, B., Biçim, G., Mahmoud, H., Dahan, I., Yalçın, A.S., Mahajna, J., Milisav, I., 2020. The potential use of natural products to negate hepatic, renal and neuronal toxicity induced by cancer therapeutics. Biochem. Pharmacol. 173, 113551. https://doi.org/10.1016/j.bcp.2019.06.007.

Purushothaman, P., Someshwar Rao, M., Rawat, Y.S., et al., 2014. Evaluation of hydrogeochemistry and water quality in Bist-Doab region, Punjab, India. Environ. Earth Sci. 72, 693–706. https://doi.org/10.1007/s12665-013-2992-9.

Quadri, J.A., Sarwar, S., Sinha, A., Kalaivani, M., Dinda, A.K., Bagga, A., Roy, T.S., Das, T.K., Shariff, A., 2018. Fluoride-associated ultrastructural changes and apoptosis in human renal tubule: a pilot study. Hum. Exp. Toxicol. 37 (11), 1199–1206.

Rajkumar, H., Dewangan, R.K., Naik, P.K., Verma, J.R., Naik, P.K., 2025b. Groundwater usage characterization in a tribal stretch infected with chronic kidney disease of unknown etiology (CKDu). J. Environ. Sci. https://doi.org/10.1016/j.jes.2025.02.037.

Rajkumar, H., Naik, P.K., Dewangan, R.K., Verma, J.R., Naik, P.K., 2025a. Hydrogeochemical forecasting in a tribal stretch infected with chronic kidney disease of unknown etiology. Sci. Total Environ. 969, 178906. https://doi.org/10.1016/j.scitotenv.2025.178906.

Rajkumar, H., Naik, P.K., Rishi, M., 2022. A comprehensive water quality index based on analytical hierarchy process. Ecol. Indic. 145, 109582. https://doi.org/10.1016/j.ecolind.2022.109582.

Rajkumar, H., Naik, P.K., Singh, G., Rishi, M., 2023. Hydrogeochemical characterization, multi-exposure deterministic and probabilistic health hazard evaluation in groundwater in parts of Northern India. Toxin Rev. 42 (1), 204–227. https://doi.org/10.1080/15569543.2022.2080222.

Ramesh, K.V., Sasibhushan, B., Gouru Naidu, K., Mohan Kumar, S., 2011. The renal failure in Uddanam Region of Srikakulam district, Andhra Pradesh: areas identified for further investigations. IUP J Chem Eng 3 (2), 68–71.

Rao, N.S., Das, R., Gugulothu, S., 2022. Understanding the factors contributing to groundwater salinity in the coastal region of Andhra Pradesh, India. J. Contam. Hydrol. 250, 104053. https://doi.org/10.1016/j.jconhyd.2022.104053.
Rathore, V., Pal, R., Galhotra, A., Nayak, S., Snehalata, Jha, V., Nagarkar, N.M., 2022. Community perception of chronic kidney disease in Supebeda, Chhattisgarh. Int. J. Curr. Res. Rev. 14 (2), 23–28. https://doi.org/10.31782/IJCRR.2022.14210.
Santoyo-Sanchez, M.P., del Carmen Silva-Lucero, M., Arreola-Mendoza, L., Barbier, O.C., 2013. Effects of acute sodium fluoride exposure on kidney function, water homeostasis, and renal handling of calcium and inorganic phosphate. Biol. Trace Elem. Res. 152, 367–372.
Saxena, V.K., Ahmed, S., 2003. Inferring the chemical parameters for the dissolution of fluoride in groundwater. Environ. Geo l43, 731–736. https://doi.org/10.1007/s00254-002-0672-2.
Scholler, H., 1965. Qualitive evaluation of groundwater resources. Method. Tech. Groundw. Invest. Dev. 33, 44–52. UNESCO Water Resource SER.
Şen, Z., 2015. Practical and Applied Hydrogeology. Elsevier. https://doi.org/10.1016/C2013-0-14020-2.
Shaji, E., Sarath, K.V., Santosh, M., Krishnaprasad, P.K., Arya, B.K., Babu, M.S., 2024. Fluoride contamination in groundwater: A global review of the status, processes, challenges, and remedial measures. Geosci. Front. 15 (2), 101734. https://doi.org/10.1016/j.gsf.2023.101734.
Shi, Q., Gao, Z., Guo, H., Zeng, X., Sandanayake, S., Vithanage, M., 2023. Hydrogeochemical factors controlling the occurrence of chronic kidney disease of unknown etiology (CKDu). Environ. Geochem. Health 45 (5), 2611–2627.
Sidhu, N., Rishi, M.S., Herojeet, R.K., 2013. Groundwater quality variation with respect to aquifer dispositioning in urbanized watershed of Chandigarh, India. Int. J. Environ. Ecol. Fam. Urban Stud. 3 (2), 87–98.
Singh, C.K., Kumar, A., Shashtri, S., et al., 2017. Multivariate statistical analysis and geochemical modeling for geochemical assessment of groundwater of Delhi, India. J. Geochem. Explor. 175, 59–71. https://doi.org/10.1016/j.gexplo.2017.01.001.
Singh, G., Rishi, M.S., Herojeet, R., Kaur, L., Sharma, K., 2020a. Multivariate analysis and geochemical signatures of groundwater in the agricultural dominated taluks of Jalandhar district, Punjab, India. J. Geochem. Explor. 208, 106395. https://doi.org/10.1016/j.gexplo.2019.106395.
Singh, G., Rishi, M.S., Herojeet, R., Kaur, L., Sharma, K., 2020b. Evaluation of groundwater quality and human health risks from fluoride and nitrate in semi-arid region of northern India. Environ. Geochem. Health 42, 1833–1862. https://doi.org/10.1007/s10653-019-00449-6.
Soltan, M.E., 1998. Characterisation, classification, and evaluation of some ground water samples in upper Egypt. Chemosphere 37 (4), 735–745. https://doi.org/10.1016/S0045-6535(98)00079-4.
Sproul, G.D., 2020. Evaluation of electronegativity scales. ACS Omega 5 (20), 11585–11594. https://doi.org/10.1021/acsomega.0c00831.
Stalin, P., Purty, A.J., Abraham, G., 2020. Distribution and determinants of chronic kidney disease of unknown etiology: a brief overview. Indian J. Nephrol. 30 (4), 241–244. https://doi.org/10.4103/ijn.IJN_313_18.
Stallard, R.F., Edmond, J.M., 1983. Geochemistry of Amazon, the influence of geology and weathering environment on the dissolved load. J. Geophys. Res. 88, 9671–9688.
Subramani, T., Rajmohan, N., Elango, L., 2010. Groundwater geochemistry and identification of hydrogeochemical processes in a hard rock region, Southern India. Environ. Monit. Assess. 162, 123–137. https://doi.org/10.1007/s10661-009-0781-4.
Sunkari, E.D., Abu, M., Zango, M.S., Wani, A.M.L., 2020. Hydrogeochemical characterization and assessment of groundwater quality in the kwahu-Bombouaka group of the Voltaian Supergroup, Ghana. J. Afr. Earth Sci. 169, 103899.
Tatapudi, R.R., Rentala, S., Gullipalli, P., Komarraju, A.L., Singh, A.K., Tatapudi, V.S., Goru, K.B., Bhimarasetty, D.M., Narni, H., 2019. High prevalence of CKD of unknown etiology in Uddanam, India. Kidney Int. Rep 4 (3), 380–389.
Thilagavathi, R., Chidambaram, S., Prasanna, M.V., Thivya, C., Singaraja, C., 2012. A study on groundwater geochemistry and water quality in layered aquifers system of Pondicherry region, southeast India. Appl. Water Sci. 2, 253–269. https://doi.org/10.1007/s13201-012-0045-2.
Tiwari, K.K., Krishan, G., Prasad, G., Mondal, N.C., Bhardwaj, V., 2020. Evaluation of fluoride contamination in groundwater in a semi-arid region, Dausa District, Rajasthan, India. Groundw. Sustain. Dev. 11, 100465. https://doi.org/10.1016/j.gsd.2020.100465.
USEPA (U.S. Environmental Protection Agency), 2024. In: Secondary Drinking Water Standards: Guidance for Nuisance Chemicals. Last updated on June 14, 2024). https://www.epa.gov/sdwa/secondary-drinking-water-standards-guidance-nuisance-chemicals. (Accessed 15 November 2024).
Veron, M.H., Couble, M.L., Magloire, H., 1993. Selective inhibition of collagen synthesis by fluoride in human pulp fibroblasts in vitro. Calcif. Tissue Int. 53, 38–44.
WHO (World Health Organization), 2022. WHO guidelines for drinking water quality. Incorporating the First and Second Addenda, fourth ed. World Health Organization, pp. 1–614.
Yiamouyiannis, J., 1983. Fluoride, the Aging Factor, 6439. Health Action Press, Delaware.
Zeng, X., He, W., Guo, H., Shi, Q., Zheng, Y., Vithanage, M., Hur, J., 2022. Recognizing the groundwater related to chronic kidney disease of unknown etiology by humic-like organic matter. npj Clean Water 5 (1), 8.
Zhang, Q., Xu, P., Qian, H., 2020. Groundwater quality assessment using improved water quality index (WQI) and human health risk (HHR) evaluation in a semi-arid region of Northwest China. Expo. Health 12, 487–500. https://doi.org/10.1007/s12403-020-00345-w.
Zhou, Y., Li, P., Xue, L., Dong, Z., Li, D., 2020. Solute geochemistry and groundwater quality for drinking and irrigation purposes: a case study in Xinle City, North China. Geochemistry 80 (4), 125609. https://doi.org/10.1016/j.chemer.2020.125609.
Zhou, Z., Shi, X., Zheng, Y., Qin, Z., Xie, D., Li, Z., Guo, T., 2014. Abundance and community structure of ammonia-oxidizing bacteria and archaea in purple soil under long-term fertilization. Eur. J. Soil Biol. 60, 24–33.